Landau levels in the presence of a potential barrier

1994 J. Phys.: Condens. Matter 6 6623

(http://iopscience.iop.org/0953-8984/6/33/010)

J. Phys.: Condens. Matter 6 (1994) 6623–6636. Printed in the UK

Landau levels in the presence of a potential barrier

J M Ferreyra† and C R Proetto

Comisión Nacional de Energía Atómica, Centro Atómico Bariloche and Instituto Balseiro, 8400 Bariloche, Argentina

Received 14 April 1994

Abstract. The exact solution to the problem of electrons under the combined effect of a square potential barrier and magnetic field parallel to the interfaces has been obtained. Beyond the states associated with the presence of an isolated interface, a new family of solutions which arises from the interaction between the two interfaces has been found. Inclusion of non-parabolic effects leads to sizable corrections, and consequently they should be taken into account in a reliable quantitative calculation. Under applied bias of typical strength, the eigenvalue spectrum changes radically as compared with the zero-electric-field results.

1. Introduction

The problem of one electron subject to the combined effects of a magnetic field and potential energy discontinuities, such as those given by the band offsets of semiconductor heterostructures, admits two extreme configurations: the magnetic field is either perpendicular or parallel to the interfaces.

In the perpendicular configuration, and for the simplest case of a single isotropic parabolic conduction band, no coupling exists between the heterojunction potential along x, and the magnetic parabola in the y–z plane [1]. Accordingly, the essential effect of the magnetic field is to quantize the degrees of freedom parallel to the interface, the total energy being just the sum of longitudinal (kinetic energy along x) and transverse (bulk Landau level) components.

When the magnetic field is applied parallel to the interfaces, a more complicated and interesting situation arises, as the total effective potential along x has contributions from both the potential energy discontinuities and the magnetic field. This coupling gives rise to an eigenvalue spectrum that shows a complex pattern. Previous theoretical studies of this problem were restricted to the case of a single interface between two semi-infinite semiconductors [2–4]. However, in the light of recent experiments [5] it seems worthwhile to generalize such calculations to the case of a finite barrier, where the magnetic length and barrier width can be of comparable magnitude. The aim of this work is to provide a detailed study of this case, including effective mass discontinuities, non-parabolic effects (not considered in any of the single-interface previous works), and the effect of an electric field applied perpendicular to the interfaces.

The rest of the paper is organized as follows. In section 2 the necessary theoretical background is presented; in section 3 several simpler configurations are analytically analysed in the light of the general exact solution obtained in the previous section, and numerical results for the general case are presented. Finally, section 4 is devoted to the conclusions.

† Fellow of the Consejo Nacional de Investigaciones Cientfficas y Técnicas (CONICET).

0953-8984/94/336623+14$19.50

2. Model and exact solution

The physical system that we have in mind is an $Al_xGa_{1-x}As$ potential barrier of height V_0 and width L along x, between two semi-infinite layers of GaAs; a magnetic field is applied along z, parallel to the interfaces between the two semiconductors.

Within the framework of the envelope wavefunction approximation of the effective mass theory [6], the behaviour of a conduction electron under the combined effect of potential energy discontinuities and magnetic fields is described by the Schrödinger equation

$$H\psi(r) = E\psi(r) \tag{1a}$$

with a Hamiltonian

$$H = \frac{p_x^2}{2m_i} + \frac{1}{2m_i}\left(p_y + \frac{e}{c}Bx\right)^2 + \frac{p_z^2}{2m_i} + V_0\,\theta[x(L-x)] - eFx \tag{1b}$$

where $m_i = m_1$ in the semi-infinite regions ($x < 0, x > L$), and $m_i = m_2$ in the barrier region ($0 < x < L$), m_1 and m_2 being the respective isotropic effective masses of the semi-infinite and barrier acting semiconductors, respectively. In writing (1) we have introduced the Landau vector potential $A = (0, Bx, 0)$ to describe the magnetic field, and an electric field of strength F along x; e is the absolute value of the electron charge and $\theta(x)$ the Heaviside step function. In principle, H should also include a term related to the spin Zeeman splitting; this will add a constant to the energy eigenvalues derived below. However, as this contribution is quite small compared with these energies (at most one per cent), we disregard it.

Since the commutators $[p_y, H] = [p_z, H] = 0$, the solution of (1) can be written as the product of plane waves along y and z, times a function $\phi(x)$ which satisfies the following effective one-dimensional equation:

$$\left(\frac{p_x^2}{2m_i} + V_0\,\theta[x(L-x)] + \frac{e^2B^2}{2c^2m_i}(x-x_i)^2\right)\phi(x) = \left(E - \frac{\hbar^2k_z^2}{2m_i} - \frac{\hbar k_y cF}{B} + \frac{m_ic^2F^2}{2B^2}\right)\phi(x) \tag{2}$$

with $x_i = x_0 + m_ic^2F/eB^2$, $x_0 = -\hbar k_y c/eB$ being the zero electric field guiding-centre coordinate [7], and k_y, k_z the wave numbers of the plane wave motion in the y–z plane. For the homogeneous bulk configuration $m_1 = m_2 = m_0$ (m_0 being the conduction-band bottom effective mass of the semi-infinite layer) and $V_0 = F = 0$, the eigenenergies of (2) are given by the well known Landau levels

$$(\tfrac{1}{2} + n)\hbar\omega_c + \frac{\hbar^2k_z^2}{2m_0} \qquad n = 0, 1, 2, \ldots \tag{3}$$

where $\omega_c = eB/m_0c$ is the cyclotron frequency. The associated eigenfunctions are the Hermite polynomials centred at x_0 [8], which have appreciable amplitude in a region of width $\sqrt{(2n+1)}\,l_B$, where $l_B = \sqrt{c\hbar/eB}$ is the magnetic length.

It is important to realize that in the absence of effective mass discontinuities, barriers, and electric fields the eigenvalues given by (3) are independent of x_0, giving rise to the well known degeneracy of the bulk Landau levels relative to this guiding-centre coordinate. However, as soon as the translational symmetry along x is lost, this degeneracy is lifted, and each eigenvalue of (2) becomes x_0 dependent. This is the problem that we want to

address in this work, for the particular case of a loss of translational symmetry due to the presence of a potential barrier.

Using $\alpha = \sqrt{2}(x - x_1)/l_B$, $\beta = \sqrt{2}(x - x_2)/l_B$, and $\hbar\omega_c$ as the unit of energy, equation (2) can be rewritten in the dimensionless form

$$\frac{d^2}{d\alpha^2}\phi(\alpha) - \left(\tfrac{1}{4}\alpha^2 - \frac{m_1}{m_0}\varepsilon_1\right)\phi(\alpha) = 0 \tag{4a}$$

if $\alpha \leqslant \alpha_0 \equiv -\sqrt{2}x_1/l_B$ (zone I) or $\alpha \geqslant \alpha_L \equiv \sqrt{2}(L - x_1)/l_B$ (zone III), and

$$\frac{d^2}{d\beta^2}\phi(\beta) - \left(\tfrac{1}{4}\beta^2 - \frac{m_2}{m_0}(\varepsilon_2 - v_0)\right)\phi(\beta) = 0 \tag{4b}$$

if $\beta_0 \leqslant \beta \leqslant \beta_L$ (zone II), with $\beta_0 \equiv -\sqrt{2}x_2/l_B$, $\beta_L \equiv \sqrt{2}(L - x_2)/l_B$. In (4*a*) and (4*b*)

$$\varepsilon_i = \left(E - \frac{\hbar^2 k_z^2}{2m_i} - \frac{\hbar k_y c F}{B} + \frac{m_i c^2 F^2}{2B^2}\right)(\hbar\omega_c)^{-1} \tag{5}$$

and $v_0 = V_0/\hbar\omega_c$. The boundary condition $\phi(x) \to 0$ as $x \to \pm\infty$ implies that we must seek solutions of (4*a*) which vanish as $\alpha \to \pm\infty$. The exact solution of (4*a*) and (4*b*) that satisfies this condition is a linear combination of the parabolic cylinder functions U and V [9] in each of the three zones

$$\phi^{I}(\alpha) = AU(a, -\alpha) \tag{6a}$$

$$\phi^{II}(\beta) = BU(b, \beta) + CV(b, \beta) \tag{6b}$$

$$\phi^{III}(\alpha) = DU(a, \alpha) \tag{6c}$$

where $a = -m_1\varepsilon_1/m_0$, $b = -m_2(\varepsilon_2 - v_0)/m_0$, and A, B, C, D are coefficients to be determined from the remaining boundary and normalization conditions.

Demanding continuity of the wavefunction at each interface, and using the boundary condition for the derivative of ϕ which ensures the conservation of the probability current across each interface [10, 11], we get a homogeneous system of four equations whose non-trivial solutions satisfy the following eigenvalue equation

$$\begin{aligned}
&m_1^2\Gamma(\tfrac{1}{2}+b)U(a,-\alpha_0)U(a,\alpha_L)[U'(b,\beta_0)U'(b,-\beta_L)\\
&\quad - U'(b,-\beta_0)U'(b,\beta_L)]\\
&\quad + m_1m_2\Gamma(\tfrac{1}{2}+b)\{U(a,-\alpha_0)U'(a,\alpha_L)[U(b,\beta_L)U'(b,-\beta_0)\\
&\quad - U'(b,\beta_0)U(b,-\beta_L)]\\
&\quad + U'(a,-\alpha_0)U(a,\alpha_L)[U'(b,\beta_L)U(b,-\beta_0) - U(b,\beta_0)U'(b,-\beta_L)]\}\\
&\quad + m_2^2\Gamma(\tfrac{1}{2}+b)U'(a,-\alpha_0)U'(a,\alpha_L)[U(b,\beta_0)U(b,-\beta_L)\\
&\quad - U(b,\beta_L)U(b,-\beta_0)] = 0.
\end{aligned} \tag{7}$$

The primes in (7) denote derivatives with respect to the second argument (excluding the sign) of the parabolic functions and the factor $\Gamma(\frac{1}{2}+b)$ represents the gamma function of argument $\frac{1}{2}+b$. The exact eigenvalue (7) is the main result of this work, and the next section will be devoted to a careful analytic and numerical analysis of its solutions. At this point we just want to point out that as is evident from the geometry of our

system, the solutions should be invariant under the simultaneous change $x_0 \to L - x_0$ and $F \to -F$. According to our definitions of α_0, α_L, β_0, and β_L this in turn implies $\alpha_0 \to -\alpha_L$, $\alpha_L \to -\alpha_0$, $\beta_0 \to -\beta_L$, $\beta_L \to -\beta_0$. It is easily checked that (7) is invariant under this symmetry operation. No simplification is evident for the equal mass case $m_1 = m_2$.

Considering that the energies involved could be well above the conduction band minimum (this is particularly true for the semi-infinite layers), we have included non-parabolic effects in the analysis. Within our scheme of calculation, we found it convenient to introduce the non-parabolic effects by using an energy-dependent effective mass. Following Lassnig [12], we employ

$$\frac{m_0}{m_i(E)} = 1 + C_m + \frac{P_v^2}{3}\left(\frac{2}{N_i + E} + \frac{1}{M_i + E}\right) - \frac{P_c^2}{2}\left(\frac{2}{N_i' - E} + \frac{1}{M_i' - E}\right) \qquad i = 1, 2. \tag{8}$$

Table 1. Values of the parameters (all in eV) which enter the evaluation of the non-parabolic corrections to the effective mass [12].

	N_i	M_i	N_i'	M_i'
$i = 1$ (GaAs)	1.519	1.860	3.140	2.969
$i = 2$ ($Al_{0.3}Ga_{0.7}As$)	1.652	1.962	3.090	2.919

This expression arises from a five-level $k \cdot p$ theory for conduction band electrons in heterostructures, with the influence of the remaining energy bands included in the constant factor C_m. For the particular case at hand, $C_m = -1.8$ and the momentum matrix elements P_v^2 and P_c^2 take the values 28.9 eV and 6 eV, respectively. The values of the parameters N_i, M_i, N_i', and M_i' for GaAs ($i = 1$) and $Al_xGa_{1-x}As$ ($i = 2, x = 0.3$) are given in table 1. It may easily be checked that for $E = 0$ (bottom of the GaAs conduction band) and for $E = 0.248$ eV (bottom of the $Al_{0.3}Ga_{0.7}As$ conduction band), the effective masses $m_1(0)$ and $m_2(0.248\,\text{eV})$ take the accepted values of $0.067m_0$ and $0.086m_0$, respectively. The important point to realize is that for all the relevant energies, the non-parabolic effective masses given by (8) are heavier than their parabolic counterparts, the corrections being larger as E increases relative to the corresponding band-edge.

The advantage of this treatment of non-parabolic effects lies in the fact that even in this case the eigenvalue equation is given by expression (7), but with the understanding that m_1 and m_2 should be obtained from the energy-dependent expression (8). This provides an additional energy contribution to (7) that can be handled without difficulty when searching for its numerical solutions.

The practical evaluation of the parabolic cylinder functions $U(a, x)$ and $V(a, x)$ poses a difficult task, which we overcome by using a combination of ascending series and asymptotic expansions in the half-plane $x > 0$ [9]. The corresponding functions in the half-plane $x < 0$ were obtained by reflection with respect to the a axis in the a–x plane. The Wronskian relation (see (10) below) satisfied by $U(a, x)$ and $V(a, x)$ proves quite useful in checking the accuracy of these expansions.

3. Analytic and numerical results

Before proceeding with the detailed numerical solution of the eigenvalue (7), it is quite illuminating to analyse limiting and simpler configurations. For example, when $L \to 0$ (vanishing small barrier width), $\alpha_L \to \alpha_0$, $\beta_L \to \beta_0$ and the only term that survives in (7) is one proportional to $m_1 m_2$. The factor may be rewritten as

$$\Gamma(\tfrac{1}{2}+b)[U(a,\alpha_0)U'(a,-\alpha_0) - U(a,-\alpha_0)U'(a,\alpha_0)] \times [U(b,\beta_0)U'(b,-\beta_0) - U(b,-\beta_0)U'(b,\beta_0)] = 0. \tag{9}$$

This equation simplifies considerably by using the Wronskian relation

$$U(a,x)U'(a,-x) - U(a,-x)U'(a,x) = \frac{\sqrt{2\pi}}{\Gamma\left(\frac{1}{2}+a\right)} \tag{10}$$

satisfied by $U(a,x)$ and $U(a,-x)$ [9]. Replacing (10) in (9) we obtain

$$\frac{1}{\Gamma(\frac{1}{2}+a)} = 0 \tag{11}$$

so the eigenvalues are determined by the poles of $\Gamma(1/2+a)$. Remembering that the gamma function diverges when its argument is a negative integer (or zero), the eigenvalues are given by the condition

$$\frac{1}{2} - \frac{m_1}{m_0}\varepsilon_1 = -n$$

which, using (5), implies

$$E_n(x_0) = \frac{eB}{m_1 c}(\tfrac{1}{2}+n) + \frac{\hbar k_z^2}{2m_1} - eFx_0 - \frac{m_1 c^2 F^2}{2B^2} \qquad n = 0, 1, 2, \ldots \tag{12}$$

as corresponds to the levels of a free electron gas in crossed electric and magnetic fields. Note the lifting of the x_0 degeneracy due to the electric field breaking of the translational symmetry, and also that when $F = 0$, (12) reduces to the result given by (3). This limit justifies the presence of the common factor $\Gamma(1/2+b)$ in (9) (and in (7)): while the gamma function has no zeros and consequently adds no solutions to (9), its presence is important in cancelling divergences in the denominator that otherwise would give rise to spurious solutions. In a very similar way one finds that an equivalent result is obtained when analysing the case $m_1 = m_2$ and $V_0 \to 0$ of (7).

As a final example, we now study the limit $L \to \infty$ of (7). From the asymptotic expansions of $U(a,\alpha_L)$, $U(b,\beta_L)$, $U(b,-\beta_L)$ and their derivatives when $\alpha_L, \beta_L \to \infty$ [9], it is easy to see that the only remaining terms of (7) are those in which there appears a product of the type $U(a,\alpha_L)U'(b,-\beta_L)$ or $U'(a,\alpha_L)U(b,-\beta_L)$. Collecting these terms we obtain

$$(m_1^2 + m_1 m_2)U(a,-\alpha_0)U'(b,\beta_0) - (m_2^2 + m_1 m_2)U'(a,-\alpha_0)U(b,\beta_0) = 0 \tag{13}$$

as the eigenvalue equation for the $L \to \infty$ limit of non-interacting interfaces. Taking $m_1 = m_2$, equation (13) reduces to the result obtained in [2, 3], while the particular case $m_1/m_2 = 0.7$ was studied in [4].

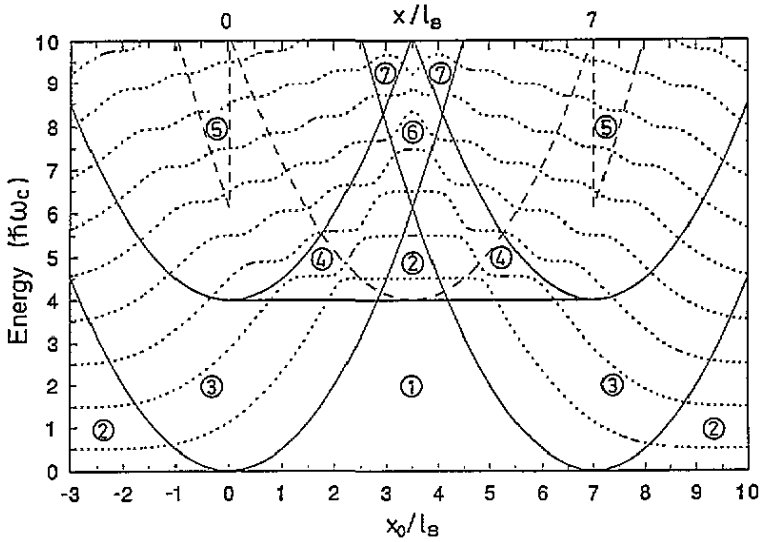

Figure 1. Lowest eigenvalues (dotted curves) as a function of the guiding-centre coordinate x_0 for a barrier width $L/l_B = 7$, with the left (right) interface at $x/l_B = 0$ (7); $v_0 = 4$ and $m_1/m_2 = 1$. Four parabolas (full curves) divide this energy-orbit centre phase space into several regions, with a different physical process taking place inside each of them. The processes are explained in the text. The broken curve corresponds to the effective potential felt by an electron with $x_0 = L/2$ (barrier centre); note that for this curve, the upper horizontal axis should be used.

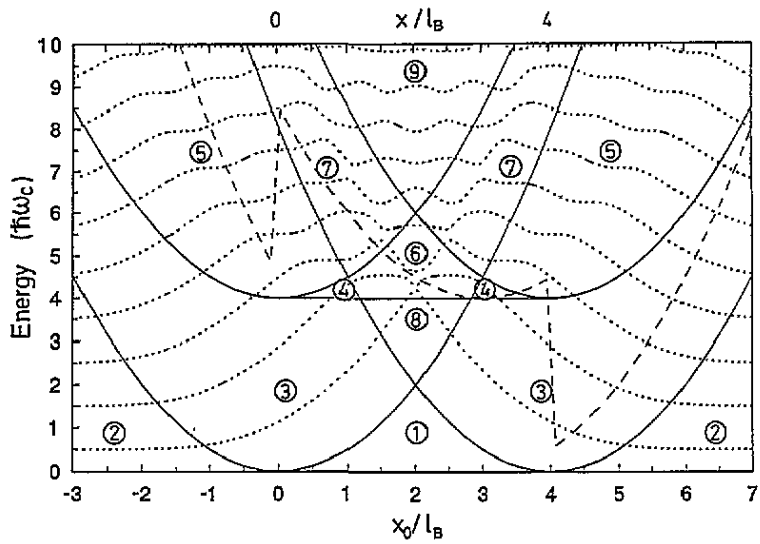

Figure 2. Same as figure 1, but for a barrier width $L/l_B = 4$; the left (right) interface lies at $x/l_B = 0$ (4). The effective potential (broken curve) corresponds to $x_0 = 3L/4$.

Turning to the numerical results, we show in figures 1–3 the lowest eigenvalues $E_n(x_0/l_B)$ of (7) as functions of x_0/l_B (dotted curves), for the simplest case $m_2/m_1 = 1$, $F = 0$, and $L/l_B = 7$, 4 and 1, respectively. Unless otherwise stated, the potential

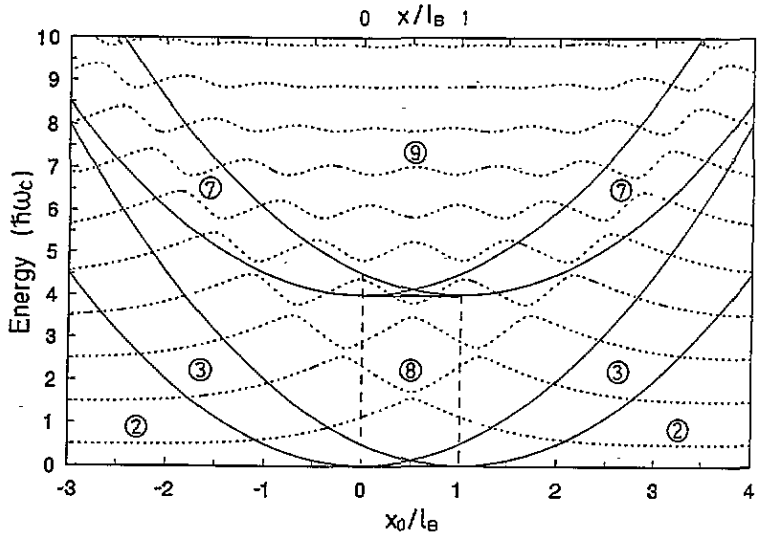

Figure 3. Same as figure 1, but for a barrier width $L/l_B = 1$, and interfaces at $x/l_B = 0$ and 1. The effective potential (broken curve) corresponds to $x_0 = L$.

barrier height $v_0 = 4$ in this work. From the relation $V_0/\hbar\omega_c = 4$, with $V_0 = 0.248\,\text{eV}$ we obtain $\hbar\omega_c = 0.062\,\text{eV}$ and consequently $B \simeq 35\,\text{T}$, a rather high but not physically unrealistic magnetic field [13]. This energy-orbit centre phase space is divided into several regions by the four parabolas $x_0^2/2l_B^2$ (full curves) centred at the bottom and top of the two interfaces. The complex pattern shown by the eigenvalues is a consequence of the fact that a different type of physical process is operative inside each region. To understand this, we have superimposed on the almost uncoupled interface results of figure 1 the effective potential (broken curve) felt by an electron when x_0 is at the barrier centre $L/2$. Clearly, the range of energies between 0 and v_0 is forbidden (region 1); when the energy is between v_0 and $(L/2l_B)^2/2$ the existence of barrier bulk Landau levels is possible (region 2), and for energies greater than range $(L/2l_B)^2/2$ but lower than $(L/2l_B)^2/2+v_0$ interface levels from the left interact with interface levels from the right mediated by levels inside the barrier zone (region 6).

Other regions can be understood from the results for the intermediate-coupled interfaces of figure 2, where the effective potential corresponds to $x_0 = 3L/4$. The forbidden region now extends between 0 and $(L/4l_B)^2/2$, but between this energy and v_0 the electrons feel an edge potential only and we have the interface states (region 3). In the narrow range between v_0 and $v_0 + (L/4l_B)^2/2$ the interaction between interface states and levels in the barrier is possible (region 4). Note that this region (and the interference mentioned above) is quite prominent in figure 1. For energies larger than $v_0 + (L/4l_B)^2/2$ but smaller than $v_0+(3L/4l_B)^2/2$ (region 7) interface levels from the left interact with levels given essentially by the mixing of interface and barrier states at the right interface. For even higher energies, region 9, we obtain a complicated interference of levels above the barrier, with a strong coupling between the two interfaces.

Figure 3 corresponds to the case $L/l_B = 1$ of strong-coupled interfaces. From the effective potential felt by the electrons when x_0 is just at the right interface, it is easy to see that the situation is quite favourable for quantum-mechanical tunnelling from an interface state from the left to a right interface state at approximately the same energy; this defines

the interface–interface region 8.

It should be pointed out here that regions 1–5 correspond to physical processes where only one interface is involved, and have already been identified in [3]. On the other hand, in regions 6–9 both interfaces are involved, and obviously these states were absent from the previous studies. The importance of these processes increases when the ratio L/l_B decreases, as can be seen clearly from the increasing size of the interface–interface against single-interface regions as one moves from figure 1 to figure 3.

Further insight into the different physical processes for each region is provided in figures 4–6, where the three lowest normalized eigenfunctions are plotted, for L/l_B = 7, 4 and 1, respectively. In each of these figures, the lower panel corresponds to $x_0 = L/2$ (barrier centre), while the upper panel to the case $x_0 = 0$ (left interface).

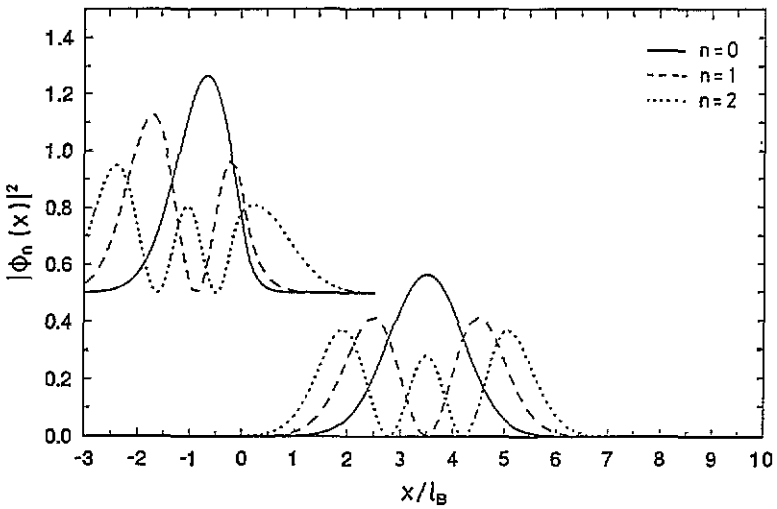

Figure 4. Three lowest normalized squared eigenfunctions for the barrier of figure 1, with $x_0 = 0$ (upper panel) and $x_0 = L/2$ (lower panel). The upper panel has been shifted upwards to avoid superposition.

According to the energy-orbit centre phase space of figure 1, the two lowest barrier-centre eigenfunctions should be close to bulk Landau orbitals, while the third level must exhibit some contribution from the interfaces. This is qualitatively supported by the lower panel of figure 4, where the three eigenfunctions look quite similar to the three lowest solutions of the one-dimensional harmonic oscillator. Note, however, that the $n = 2$ eigenfunction almost reaches the interfaces, and consequently the bulk Landau level is barely defined, as can be seen from figure 1. The upper panel, corresponding to the $x_0 = 0$ three lowest eigenfunctions, shows how a well defined interface level ($n = 0$) evolves towards a reflection interference level ($n = 2$, region 5 in figure 1) with a sizable probability of finding the electron in the barrier region.

Quite different is the situation shown in the lower panel of figure 5, as compared with the equivalent barrier-centre eigenfunctions of the previous case. The well defined bulk Landau levels, with almost all the weight in the barrier region, have been replaced by interface states connected by tunnelling below and above the barrier (regions 8 and 6 of figure 2, respectively). Note, however, that the $n = 2$ wavefunction still has an appreciable probability of being at the barrier, which explains the fact that $E_2(L/2l_B)$ takes a value close

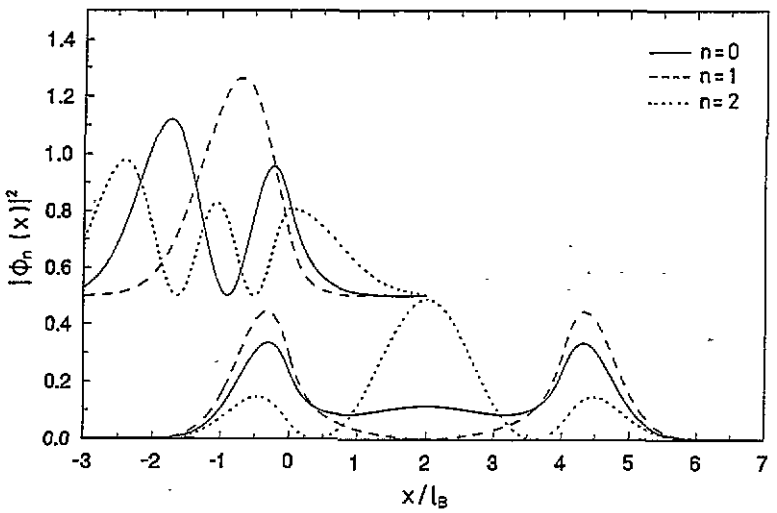

Figure 5. Three lowest normalized squared eigenfunctions for the barrier of figure 2, with $x_0 = 0$ (upper panel), and $x_0 = L/2$ (lower panel).

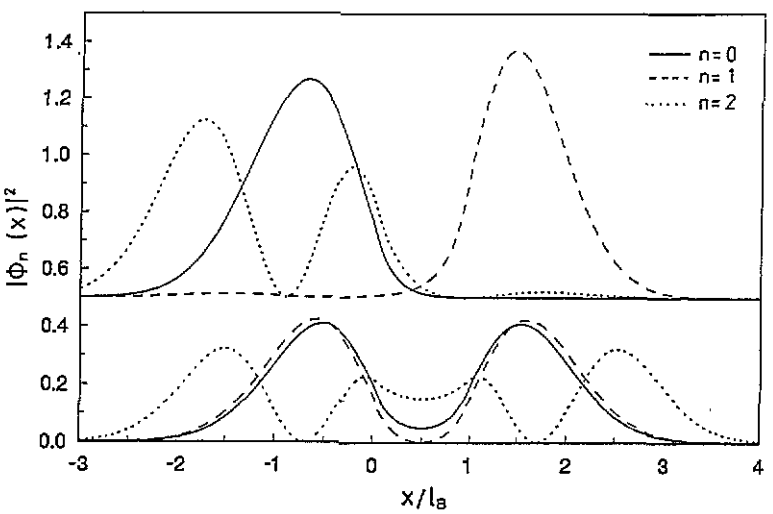

Figure 6. Three lowest normalized squared eigenfunctions for the barrier of figure 3, with $x_0 = 0$ (upper panel), and $x_0 = L/2$ (lower panel).

to 4.5, the eigenvalue corresponding to a bulk Landau level in the barrier. No important difference could be observed between the upper panels of figures 4 and 5, as in both cases these states are in the non-interacting interface region of their respective energy-orbit centre phase space.

The situation changes again radically for the thinner barrier with $L/l_B = 1$, as shown in figure 6. For both $x_0 = 0$ and $L/2$ we are in the interface–interface region mediated by tunnelling below the barrier (region 8) of figure 3. This is seen clearly from the lower panel, where the probability is strongly peaked close to the interfaces, with a much smaller probability at the barrier centre (this is particularly true for the two lowest eigenstates).

From the upper panel, however, it is evident that when these eigenfunctions are inside region 8, and far from the anticrossing points, the eigenfunctions are essentially interface levels on the left ($n = 0$ and 2), or interface levels on the right ($n = 1$). It is quite noticeable that keeping the orbit centre parameter x_0 constant at one interface, one can obtain a wavefunction localized at the opposite interface just by changing the eigenvalue.

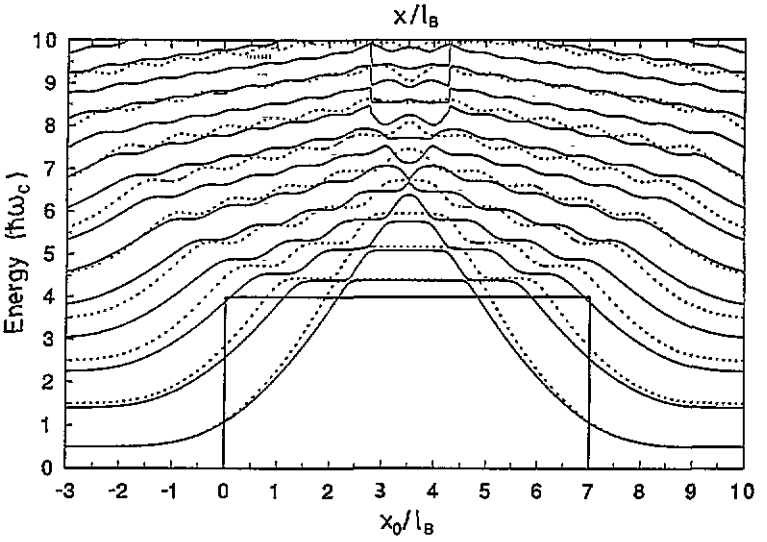

Figure 7. Lowest eigenvalues as a function of the guiding-centre coordinate x_0 for a barrier with $L/l_B = 7$, $v_0 = 4$. Full thin curve, energy-dependent effective masses; broken curve, $m_1/m_2 = 0.067/0.086$. The upper horizontal axis corresponds to the thick full curve, which represents the potential barrier.

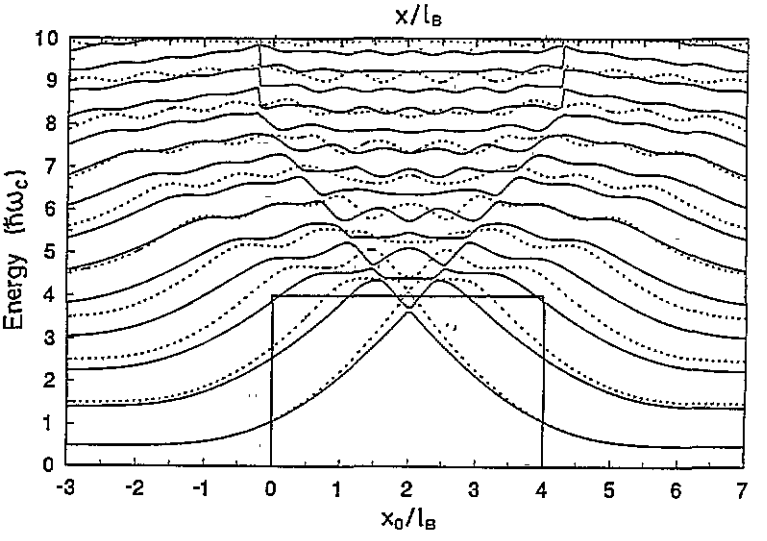

Figure 8. Same as figure 7 for a barrier with $L/l_B = 4$.

Once the qualitative behaviour of the complex pattern of figures 1–3 has been understood, we include non-parabolicity in the calculations. The results are shown in figure 7 for the case $L/l_B = 7$ and in figure 8 for $L/l_B = 4$. The full curve corresponds to the energy-dependent effective masses given by (8), and the dotted curve to the constant ratio $m_1/m_2 = 0.067/0.086 \simeq 0.78$.

A first feature to note from figures 7 and 8 is the decrease of the energy splitting between successive solutions, from about $\hbar\omega_c$ in the GaAs regions to about $\hbar\omega_c m_1/m_2$ ($< \hbar\omega_c$) in the $Al_xGa_{1-x}As$ regions; this is particularly clear in the regions where bulk Landau levels are well defined. Note also that the non-parabolic levels lie always below the corresponding parabolic levels. This should be expected, as the energy-dependent effective masses of (8) are increasing functions of energy, and also from the m^{-1} dependence of the Landau levels in each of the bulk materials.

For a given solution, the importance of the non-parabolic corrections depends on its character (bulk Landau, interface, etc). Focusing on the lowest eigenvalue of figure 7, for example, the correction is negligible when $-x_0/l_B \gg 1$ (far left) or $(x_0 - L)/l_B \gg 1$ (far right), where it behaves as a bulk Landau level. But when x_0 is at a distance of about l_B from any of the interfaces, and the level starts to behave as an interface state, the corrections are quite sizable. However, the correction again becomes negligible in the barrier region, as the electron is now very close to the bottom of the $Al_xGa_{1-x}As$ conduction band, where non-parabolic effects are quite small. This should be contrasted with the behaviour of the lowest solution of figure 8, where the non-parabolic corrections are a maximum just at the barrier centre, as a result of the interface character of this state when $x_0 = L/2$. In both cases, for excited states the energy-dependent effective masses give sizable contributions over the whole range of x_0. This explains the fact that, for a given energy range, there are many more non-parabolic solutions than parabolic ones (14 against nine solutions for $x_0 = L/2$ in figure 8, for instance). From the results, it is clear that non-parabolic corrections should be included in a reliable quantitative calculation of the perturbed Landau levels close to a square barrier.

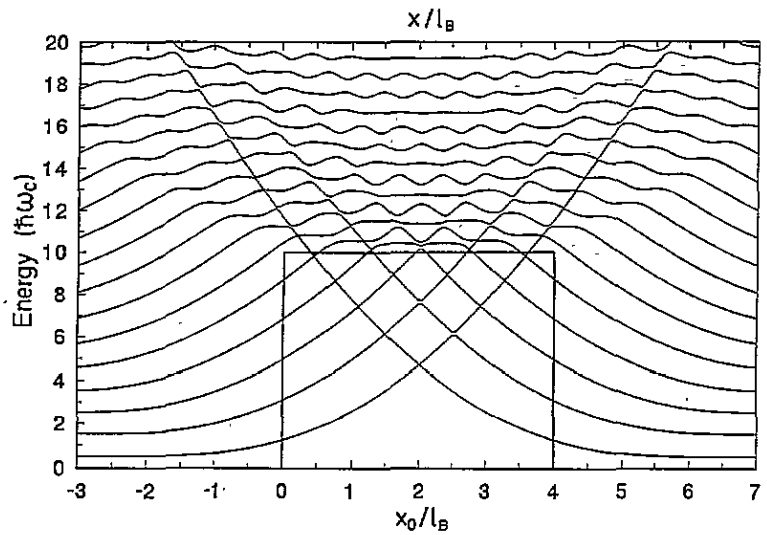

Figure 9. Zero-electric-field eigenvalues versus x_0 for a barrier with $v_0 = 10$ and $L/l_B = 4$. The thick full curve represents the potential barrier.

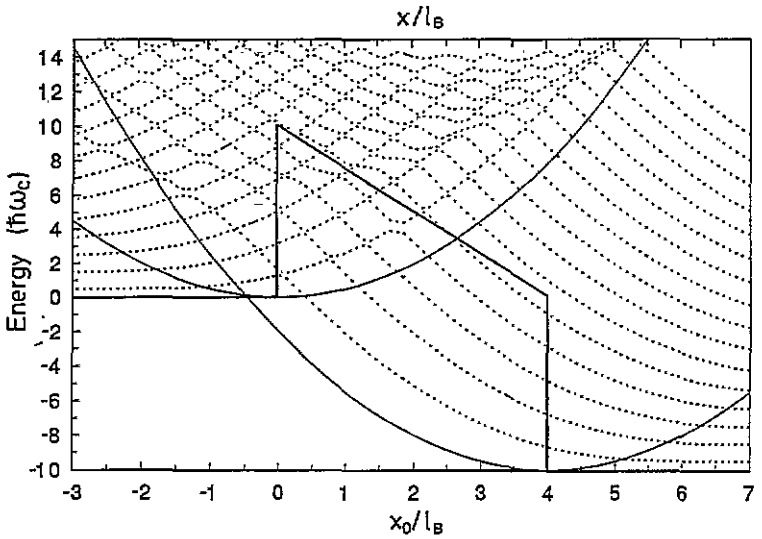

Figure 10. Eigenvalues under applied bias for the barrier of figure 9. The electric field strength $F = 2.5F_0$ (F_0 is defined in the text). Also shown are the two parabolas centred at the bottom of each interface, and the potential barrier under bias.

All the results presented up to now were obtained in the absence of electric field effects; we give in figures 9 and 10 an example of the modifications introduced by an applied bias. The barrier height and width are $v_0 = 10$ and $L/l_B = 4$, and are typical for the experiments of [5]. Figure 9 corresponds to the zero-electric-field case, and the results should be compared with figures 2 and 8, corresponding to barriers of similar width but smaller v_0. Note the increased number of interface–interface states, as a consequence of the larger size of region 8, where these states exist.

Defining the electric field unit from the relation $eF_0l_B = \hbar\omega_c$, the results presented in figure 10 correspond to $F = 2.5F_0$. For a barrier with $V_0 = 0.248\,\mathrm{eV}$, and from $v_0 = 10$, we obtain $B \simeq 15\,\mathrm{T}$ and $F_0 \simeq 3.7 \times 10^4\,\mathrm{V\,cm^{-1}}$. Keeping in mind that in most of the experiments the two semi-infinite layers are heavily doped with donor impurities, whose released electrons screen quite effectively the applied fields, we have assumed that all the bias drops at the potential barrier region. Self-consistent calculations for similar double-barrier tunnelling devices show that this is a good approximation [14]. For the particular field strength $F = 2.5F_0$, the upper corner of the right interface lies at the same energy as the lower corner of the left interface.

A comparison between figures 9 and 10 shows that in the presence of an applied bias, the left-interface states are 'squeezed' into a small region, while about half of the displayed spectra correspond now to right-interface states. Note, for example, that for $x_0/l_B = 4$ (right interface) one finds interface states above the upper corner of the barrier, while when $F = 0$, at energies above v_0 one finds region 5, corresponding to reflection-interference levels (see figure 2). The reason for this is obvious: by increasing F, the slope of the potential barrier (between 0 and L) also increases, and it behaves as an effective interface, giving rise to an extended region of interface states. Precisely the opposite occurs at the left interface, where the triangular potential and its associated tunnelling transparency make this interface progressively lose the interface character.

4. Conclusions

The exact eigenvalue equation for conduction electrons subject to potential barriers, magnetic field parallel to the interfaces, and applied bias along the growth direction, has been derived. Its solutions can be obtained analytically in several limiting and simpler cases, while the general case must be studied numerically.

The solutions exhibit a complex pattern as a function of the guiding-centre coordinate, even in the simplest case of parabolic bands, equal semi-infinite layer and barrier effective masses and zero electric field. Beyond the states associated with the presence of an isolated interface, we have found a new family of solutions, which arises from the interaction between the two interfaces. The relevance of the latter solutions increases when the ratio L/l_B between the barrier size and magnetic length decreases. The analysis is greatly simplified by drawing four parabolas (two at each interface, one at the bottom corner, one at the upper corner) which divide the energy-orbit centre phase space into several regions, each of which corresponds to a different physical process. The analysis of the exact wavefunctions also proves useful, as they give a real-space insight into the nature of the solutions. In particular, we have found that even when fixing the orbit centre parameter x_0 at one interface, it is possible to obtain a wavefunction quite localized at the opposite interface, just by changing the eigenvalues.

Having acquired a qualitative understanding of the energy-orbit centre phase space, we included non-parabolic effects by using an energy-dependent effective mass; the corrections turned out to be important, particularly in the GaAs regions and for interface states. They should clearly be incorporated into any theoretical calculation aiming to provide reliable quantitative information on this problem.

Under applied bias of typical strength, important changes of the eigenvalue spectra are obtained. The tilted potential barrier between 0 and L behaves effectively as an extended interface for right-interface states, while it behaves like a triangular barrier for the left-interface states. Accordingly, in the energy-guiding centre phase space under bias, the right-interface region increases, while the left-interface region decreases.

A proper comparison with available experimental results on the perturbed Landau levels close to a GaAs barrier will require a calculation of the tunnelling current under applied bias [15–17], including self-consistent screening, effective mass discontinuities, and non-parabolic effects. Work in this direction is underway.

Acknowledgments

One of us (JMF) is indebted to the CONICET of Argentina for financial support. The authors wish to thank V Grunfeld for a careful reading of the manuscript.

References

[1] Bastard G 1988 *Wave Mechanics Applied to Semiconductor Heterostructures* (Paris: Editions de Physique)
[2] Vigneron J P and Ausloos M 1978 *Phys. Rev.* B **18** 1464
[3] Johnson E A, MacKinnon A and Geobel J C 1987 *J. Phys. C: Solid State Phys.* **20** L521
[4] Johnson E A and MacKinnon A 1988 *J. Phys. C: Solid State Phys.* **21** 3091
[5] Hickmott T W 1989 *Phys. Rev.* B **40** 8363, 11 683; 1991 *Phys. Rev.* B **44** 12 880
[6] Bastard G and Brum J 1986 *IEEE J. Quantum Electron.* **22** 1625
[7] Aoki H 1987 *Rep. Prog. Phys.* **50** 655

[8] Ziman J M 1965 *Principles of the Theory of Solids* (Cambridge: Cambridge University Press)
[9] Miller J C P 1965 *Handbook of Mathematical Functions* ed M Abramowitz and I A Stegun (New York: Dover) ch 19
[10] BenDaniel D J and Duke C B 1966 *Phys. Rev.* **152** 683
[11] Bastard G 1981 *Phys. Rev.* B **24** 5693
[12] Lassnig R 1985 *Phys. Rev.* B **31** 8076
[13] Miura N, Yamada K, Kamata N, Osada T and Eaves L 1991 *Superlatt. Microstruct.* **4** 527
[14] Sofo J O and Balseiro C A 1990 *Phys. Rev.* B **42** 7292
[15] Brey L, Platero G and Tejedor C 1988 *Phys. Rev.* B **38** 9649
[16] Schulz P A and Tejedor C 1989 *Phys. Rev.* B **39** 11 187
[17] Platero G, Schulz P A, Brey L and Tejedor C 1990 *Surf. Sci.* **228** 291